Analyzing astrophysical neutrino signals using realistic nuclear structure calculations and the convolution procedure

V. Tsakstara*
Division of Theoretical Physics, University of Ioannina, GR-45110 Ioannina, Greece

T. S Kosmas†
Institut für Kernphysik Technische Universität Darmstadt, DE-64289 Darmstadt, Germany, and GSI, Theoretical Physics Division, DE-64291 Darmstadt, Germany

(Received 5 September 2011; revised manuscript received 21 October 2011; published 29 December 2011)

Convoluted differential and total cross sections of inelastic ν scattering on ^{128,130}Te isotopes are computed from the original cross sections calculated previously using the quasiparticle random-phase approximation. We adopt various spectral distributions for the neutrino energy spectra such as the common two-parameter Fermi-Dirac and power-law distributions appropriate to explore nuclear detector responses to supernova neutrino spectra. We also concentrate on the use of low-energy β-beam neutrinos, originating from boosted β^--radioactive ^{6}He ions, to decompose original supernova (anti)neutrino spectra that are subsequently employed to simulate total cross sections of the reactions $^{130}\mathrm{Te}(\tilde{\nu}, \tilde{\nu}')^{130}\mathrm{Te}^*$. The concrete nuclear regimes selected, ^{128,130}Te, are contents of the multipurpose CUORE and COBRA rare event detectors. Our present investigation may provide useful information about the efficiency of the Te detector medium of the above experiments in their potential use in supernova neutrino searches.

DOI: 10.1103/PhysRevC.84.064620 PACS number(s): 26.50.+x, 23.40.Bw, 25.30.Pt, 97.60.Bw

I. INTRODUCTION

The physics of low-energy neutrinos, a multidisciplinary research field within astrophysics, nuclear physics, particle physics, and cosmology, has for the past few decades aroused intense interest and been at the forefront of research topics [1–4]. This field covers many aspects of fundamental interactions [1,3], nuclear astrophysics [4], nuclear structure [5–10], and neutrino detection physics [1,8]. In this light, extremely sensitive neutrino probes aiming to detect astrophysical neutrinos provide unique signals for studying stellar evolution and astrophysical reactions [1,4,11–15]. Specifically neutrino-nucleus interaction activities, which can be realized with detectors based on several target nuclei [5–10], provide valuable information about the semileptonic astrophysically important electro-weak interaction processes and they shed light on the nuclear responses in the low-energy range [4,14,15].

There is, however, a plethora of important questions associated with the weak processes occurring in the interior of distant stars [4,15], the terrestrial detection of astrophysical neutrinos [1,16–18], and supernova dynamics [19,20] that remain to be answered. This motivates significant theoretical advances in order to understand the pertinent neutrino sources in conjunction with the decisive role of neutrinos in astrophysical phenomena [12,15]. Toward this end, measurements of low-energy astrophysical neutrino fluxes, originating from collapsing stars, the Sun, and the Earth have nowadays become feasible with high statistics [16,21–25]. Also low-energy ν-nucleus cross-section measurements are now accessible at currently operating experiments and expected to operate facilities with accelerator-made neutrino sources, such as (i) low-energy β beams [26–33] and (ii) the Spallation Neutron Source (ORLaND experiment and European Spallation Source) [34–36], that exploit conventional ν sources such as π decay and μ decay at rest [37,38]. In addition, activities of extremely sensitive rare-event probes with multiple physics goals (nuclear double-β-decay and low-energy neutrino searches) have been developed that potentially may be used for neutrino detection like the MOON [1], CUORE [39,40], COBRA [41], SNO+ [42], and other experiments [3,43,44]. In point of fact, reliable interpretations of the neutrino signals created with various nuclear detectors from astrophysical as well as laboratory neutrino sources are of particular significance. The ν-nucleus interactions in such terrestrial experiments, but also in an astrophysical environment, are of primary importance to understand ν scattering inside the matter of massive stars that determines the shape of the respective neutrino energy spectra and the signals recorded in ν detectors [45–47]. Below we briefly outline some of the main known characteristics of these low-energy neutrino sources that we consider important for the purposes of our present work [16,18] (for a comprehensive discussion the reader is referred to recent reviews [1,4]).

A supernova explosion is one of the most interesting low-energy neutrino sources generating a huge number of all six flavors of neutrinos (ν_ℓ, $\tilde{\nu}_\ell$, with $\ell = e, \mu, \tau$) that scatter out of the collapsing core (a flux of 10^{58} neutrinos is emitted in about 10 s) taking away the greatest part of the gravitational binding energy released in the collapse (approximately the 98–99% of the total released energy) [11–13,45,46]. The ν_e neutrinos decouple and escape at the largest radius of the star, the $\tilde{\nu}_e$ antineutrinos decouple at an inner region, with radius smaller than that where ν_e neutrinos decouple, and the other neutrino flavors decouple deepest in the star [15,20]. The temperature T

*vtsaksta@cc.uoi.gr
†Permanent address: Department of Physics, University of Ioannina, GR-45110 Ioannina, Greece; hkosmas@uoi.gr; t.kosmas@gsi.de

(which reflects the mean energy of the specific neutrino flavor), for ν_e neutrinos is $T \approx 3.5$ MeV, for $\tilde{\nu}_e$ anti-neutrinos is $T \approx 5$ MeV, and for the other neutrino species is $T \approx 8$ MeV [15,20,45,46]. The core-collapse supernovae is a longstanding open problem but the development of neutrino facilities during the last decades (after the observation of SN1987A) ensures that when the next (extra)galactic supernova (SN) occurs a great number of different neutrino detectors being in operation will record unique information about the SN neutrino energy spectra, the mechanisms that generate them, and the conditions under which they are released from the collapsing star [20,43].

The solar neutrinos, originally conceived as a powerful tool to investigate the Sun's deep interior [48], have provided precious information to aide in the discovery of new physics and the interpretation of the profound phenomenon of neutrino oscillations [16,49,50]. Future experiments like the SNO+ are expected to contribute crucially in order to explore the CNO-cycle neutrino flux and clarify the open issue of the Sun's core metalicity [23]. On the other hand, geoneutrinos have been successfully detected by the liquid-scintillator experiments of the KamLAND [24] and Borexino [25] Collaborations, but the geological information contained in these measurements is still limited, mostly because of low statistics. The next generation detectors, like the liquid-scintillator neutrino observatory LENA [43,44], the Borexino [48], and the SNO+ [41] experiments, are expected to give useful answers to several questions of extraordinary geological importance regarding the precise geo-ν fluxes and abundances of natural radioactive elements (K, U, Th) in the Earth's interior.

In the present work, we focus on the interpretation of astrophysical ν signals generated in nuclear detectors of terrestrial experiments through the investigation of the response of the detector medium to the respective neutrino energy spectra. We emphasize those signals coming from SN neutrinos by using the following basic theoretical ingredients:

(i) The original differential and total cross sections of the neutral-current reactions $^{128,130}\mathrm{Te}(\nu, \nu')^{128,130}\mathrm{Te}^*$ and $^{128,130}\mathrm{Te}(\tilde{\nu}, \tilde{\nu}')^{128,130}\mathrm{Te}^*$ computed in Ref. [7] via realistic state-by-state calculations performed with a refinement of the quasiparticle random-phase approximation (QRPA) [7–9,51–56]. From that point of view the present paper is an extension of our recently published work [7].

(ii) Reliable descriptions of the shapes of neutrino energy distributions provided either from astrophysical numerical simulations of core-collapse SN (the well-known Fermi-Dirac and power-law distributions) [57–59] or from the parametrizations of supernova neutrino spectra based on the use of the low-energy β-beam spectra [30–33] produced from accelerated radioactive ^{6}He ion beams.

(iii) Very fast and fine computational tools for the required folding procedure in order to simulate the signal expected to be recorded on Te detectors (the detector medium of CUORE is TeO_2 and that of COBRA is CdTe or CdZnTe) from low-energy astrophysical ν sources.

The paper is structured as follows. At first (Sec. II), the main characteristics of the folding formalism in nuclear and astronuclear physics are briefly summarized. Then (Sec. III), the features of the spectral distributions of the neutrino sources of our interest, focusing on the neutrinos generated in core-collapse supernovae, are outlined. Our folded cross-section results for neutral-current neutrino and antineutrino scattering off the ^{128,130}Te isotopes are comprehensively discussed in Sec. IV, and, finally (Sec. V), the main conclusions of the present investigation are extracted.

II. BRIEF DESCRIPTION OF THE FORMALISM

The original calculations for neutral-current ν-nucleus scattering rely on the double-differential cross section [5,7–9]:

$$\frac{d^2\sigma_{i\to f}}{d\Omega d\omega}(\hat{\Omega}, \omega, \varepsilon_\nu)|_{\nu/\tilde{\nu}} = \delta(E_f - E_i - \omega)\frac{2G^2(\varepsilon_\nu - \omega)^2\cos^2(\theta/2)}{\pi(2J_i+1)} \times [\mathcal{C}_V + \mathcal{C}_A \mp \mathcal{C}_{VA}], \quad (1)$$

where $\hat{\Omega} = (\varphi, \theta)$, with θ (φ) being the polar (azimuthal) angle (in the laboratory frame) of the outgoing lepton. E_i and E_f represent the energy of the initial (ground) and final excited nuclear states of the studied nuclide and ω denotes the nuclear excitation energy, which, from the energy conservation involved in the δ function of Eq. (1), is given by

$$\omega = E_f - E_i = \varepsilon_\nu - \varepsilon_f. \quad (2)$$

ε_ν (ε_f) stands for the energy of the incoming (outgoing) lepton (the nuclear recoil is neglected). In Eq. (1), the ($-$) or ($+$) sign corresponds to scattering of neutrinos or anti-neutrinos, respectively. The polar (axial) vector contribution C_V (C_A) and the overlap polar vector–axial vector term C_{VA} involve the matrix elements of the respective ν-nucleus interaction operators (see the Appendix).

In evaluating original ν-nucleus cross sections starting from Eq. (1), it is adopted that the incoming neutrinos are monochromatic of energy ε_ν. The neutrino beams in actual experiments (pion-muon stopped neutrinos, β-beam neutrinos, reactor neutrinos, etc.) [34,35,38,60,61] and the astrophysical neutrinos of our interest (solar, supernova, geoneutrinos) [16,21–25,44] are, in general, not monoenergetic but rather have broad energy distributions (sometimes they consist of a mixture of neutrinos and antineutrinos) [16,18,23–25], characteristic of the considered source and defined as

$$\frac{dN_\nu(\varepsilon_\nu)}{d\varepsilon_\nu} \equiv \eta(\varepsilon_\nu) \quad (3)$$

(N_ν denotes the number of neutrinos of the beam). The distributions $\eta(\varepsilon_\nu)$ are usually normalized as

$$\int_0^\infty \eta(\varepsilon_\nu)d\varepsilon_\nu = 1. \quad (4)$$

Through the energy spectrum $\eta(\varepsilon_\nu)$ of a specific neutrino source, the original ν-nucleus cross sections (of neutral- and charged-current reactions) computed in the context of a nuclear model can be connected with physical observables and the signals created at the nuclear detectors by utilizing the convolution (folding) method described below.

It is important to note that, throughout the present paper only inelastic (incoherent) cross sections, original and folded ones, are considered. The coherent (elastic) channel (where an additive contribution of all nucleons of the target nucleus takes place), which is also possible through the vector current component in neutral-current ν-nucleus scattering, even though much easier to calculate, needs special treatment, both experimentally and theoretically [16,18], and is discussed elsewhere [62].

A. The convolution procedure in ν-nucleus reactions

For terrestrial experiments associated with neutrino detection through ν-nucleus interactions, the convolution (folding) of the theoretical cross sections provides an estimate of the response of the nuclear-detector to the energy distribution of the observed neutrinos. The features of the neutino-flux arriving at the detector are encoded in the nuclear response of the detector and theoretically they could be reproduced by convoluted cross section calculations [51–53,56].

The relevant formalism, specified according to the desired observable or convoluted cross section type (double-differential, single-differential, total, or cumulative) of neutrino-nucleus reactions, is outlined below.

1. Folding of double-differential cross sections

In the case of the original double-differential ν-nucleus cross section, $d^2\sigma(\theta,\omega,\varepsilon_\nu)/d\Theta d\omega$, where $d\Theta=\sin\theta d\theta$ (the integration over the azimuthal angle ϕ of Eq. (1) gives simply 2π), the convolution with a spectral distribution $\eta(\varepsilon_\nu)$ is defined by the expression [2,51–53,56]

$$\left[\frac{d^2\sigma(\theta,\omega)}{d\Theta d\omega}\right]_{\rm fold}=\int_\omega^\infty \frac{d^2\sigma(\theta,\omega,\varepsilon_\nu)}{d\Theta d\omega}\eta(\varepsilon_\nu)d\varepsilon_\nu, \qquad (5)$$

where the energy ω in the lower limit of the integral denotes that incoming neutrinos with energy ε_ν cause nuclear transitions for which $\omega\leqslant\varepsilon_\nu$.

A slightly different type of folded double-differential cross section is defined with respect to the laboratory scattering angle θ and the energy of the outgoing lepton ε_f for both categories of neutrino-nucleus reactions, the charged-current [63] and the neutral-current [64,65] ones. The corresponding expression is written as

$$\left[\frac{d^2\sigma(\theta,\varepsilon_f)}{d\Theta d\varepsilon_f}\right]_{\rm fold}=\int_{\varepsilon_{\rm thres}}^\infty \frac{d^2\sigma(\theta,\varepsilon_f,\varepsilon_\nu)}{d\Theta d\varepsilon_f}\eta(\varepsilon_\nu)d\varepsilon_\nu, \qquad (6)$$

where $\varepsilon_{\rm thres}$ denotes the energy threshold of the nuclear detector which for neutral-current ν-nucleus processes is equal to the energy of the first excited state of the target-nucleus (incoherent channel).

It is worth mentioning that, recently, at Fermilab (MiniBooNE Collaboration) [60] the muon-neutrino charged-current quasielastic double-differential cross section with respect to the final muon energy ($d^2\sigma/d\Omega d\varepsilon_f$) has been measured. This gives a special theoretical importance to the folded cross sections defined by Eqs. (5) and (6). The MiniBooNE neutrino detector is currently used for searching core-collapse supernovae in the Milky Way Galaxy [61].

2. Folding of single-differential cross sections

The information transferred by the energy spectrum of a specific neutrino source (e.g., supernova neutrinos) is concealed in the response of the nuclear detector to this neutrino spectrum which is mostly described by the folded single-differential ν-nucleus cross sections, $[d\sigma(\omega)/d\omega]_{\rm fold}$, defined as

$$\left[\frac{d\sigma(\omega)}{d\omega}\right]_{\rm fold}=\int_\omega^\infty \frac{d\sigma(\omega,\varepsilon_\nu)}{d\omega}\eta(\varepsilon_\nu)d\varepsilon_\nu, \qquad (7)$$

where $d\sigma(\omega,\varepsilon_\nu)/d\omega$ is the original single-differential cross section obtained from Eq. (1) by integrating over angles. The latter definition describes the signal recorded on the nuclear detector in the infinitesimal energy region $d\omega$ around the excitation energy ω of the nuclear detector isotope. The theoretical predictions of the excitation spectrum $[d\sigma(\omega)/d\omega]_{\rm fold}$ indicate what the neutrino signal in the detector will look like. Specifically, in the case of a supernova ν source the response obtained by Eq. (7) reflects the reaction products of ν-nucleosynthesis processes that will be encrypted in the terrestrial detector [4,14,15] (see Sec. IV for the Te isotopes).

3. Folding of total cross sections

The response of a nuclear ν detector throughout its energy spectrum as a function of the incoming neutrino energy ε_ν that is created by a specific neutrino distribution $\eta(\varepsilon_\nu)$ is written as [51]

$$\sigma_{\rm fold}(\varepsilon_\nu)=\sum_{\omega=\varepsilon_{\rm thres}}^{\omega=\varepsilon_\nu}\sigma(\omega,\varepsilon_\nu)\eta(\varepsilon_\nu). \qquad (8)$$

This means that, for the total incoherent ν-nucleus cross section $\sigma_{\rm tot}(\varepsilon_\nu)$, the signal on the detector of a neutrino spectral distribution (versus the incoming neutrino energy ε_ν), $\eta^{\rm sign}(\varepsilon_\nu)$, is evaluated by

$$\sigma^{\rm sign}_{\rm fold}(\varepsilon_\nu)=\sigma_{\rm tot}(\varepsilon_\nu)\eta^{\rm sign}(\varepsilon_\nu), \qquad (9)$$

Results based on the latter expression for the total incoherent cross sections of ν scattering on Te isotopes are presented in Sec. IV D.

III. LOW-ENERGY NEUTRINO SPECTRA

In this section we briefly summarize the main features that characterize the laboratory and astrophysical neutrino energy spectra needed for the purposes of the present work. For the interpretation of supernova neutrino spectra, $\eta_{\rm SN}(\varepsilon_\nu)$, in the astrophysical environment where they are produced but also at the terrestrial detector where they are detected, two-parameter spectral distributions of Fermi-Dirac or power-law type are commonly assumed [12,20,57–59]. However, the energy range and shape of laboratory neutrinos produced in pion-muon stopped neutrino sources roughly resembles the energey range

and shape of SN neutrinos. On the other hand, recently, linear combinations of low-energy β-beam neutrinos with different boosting Lorentz factors γ have been employed for the interpretation of SN neutrino signals recorded at the nuclear ν detectors [30,33]. In the present work we adopt this method and use laboratory ν sources in discussing SN neutrinos in Sec. IV.

A. Energy-spectra of laboratory neutrino sources

1. *Pion-muon stopped neutrino energy distributions*

At various past operating or currently running pion-muon stopped neutrino sources (LAMPF, KARMEN, MiniBooNE and BooNE, etc.) [37,38], and in the future at the Neutron Spallation Source (ORLaND experiment, European Spallation Neutron Source) [34,35], ν_e neutrinos and $\tilde{\nu}_\mu$ antineutrinos are produced from the decay of muons according to the reaction

$$\mu^+ \to e^+ + \nu_e + \tilde{\nu}_\mu. \tag{10}$$

Because the decaying muons result from the decay of slow pions ($\pi^+ \to \mu^+ + \nu_\mu$), they have relatively low energies. In these facilities, the energy spectra of ν_e neutrinos and $\tilde{\nu}_\mu$ antineutrinos are approximately described by the normalized distributions [6,14]

$$\eta_{\nu_e}(\varepsilon_\nu) = 96\varepsilon_\nu^2 M_\mu^{-4}(M_\mu - 2\varepsilon_\nu), \tag{11}$$

$$\eta_{\tilde{\nu}_\mu}(\varepsilon_\nu) = 16\varepsilon_\nu^2 M_\mu^{-4}(3M_\mu - 4\varepsilon_\nu), \tag{12}$$

where $M_\mu = 105.6$ MeV is the muon rest mass. The maximum energy of ν_e and $\tilde{\nu}_\mu$ in Eqs. (11) and (12) is $\varepsilon_\nu^{\max} = 52.8\,\text{MeV} = M_\mu/2$. It is worth noting that the pion-muon stopped neutrino beams cannot become completely pure like, for example, the β-beam neutrinos (see below). The distribution of Eq. (11) is the characteristic Michel energy spectrum. For more details the reader is referred to Refs. [1,2,6,38].

From a simulation performance point of view, the analytic expressions (11) and (12) are very convenient for the required numerical integration in the convolution procedure. On the other hand, their energy range and shape roughly resemble those of SN neutrinos. However, they are not realistic in the high-energy tail to be safely utilized for analyzing supernova neutrino signals. Alternative choices are discussed below.

2. *Low-energy β-beam neutrinos*

Recently at some facilities, some accelerated β-radioactive nuclei have been proposed as sources of neutrino- beams (β-beam neutrinos) [26–28,31]. Such facilities may produce pure beam neutrinos in which the possible flavors are either the ν_e neutrinos (for β^+-decaying ions) or the $\widetilde{\nu}_e$ antineutrinos (for β^--decaying ions) to search for standard and nonstandard neutrino physics at low and intermediate energies (ν-nucleus interactions, neutrino properties, neutrino oscillations, etc.) and measure ν-nucleus scattering cross sections [27,31].

The laboratory-frame energy distribution of these neutrinos, assuming that the decaying nuclei are moving with velocity $u = c\sqrt{\gamma^2 - 1}/\gamma$, reads [27,31,32]

$$\eta_\gamma(\varepsilon_\nu) = \frac{ln2}{m_e^5(\text{ft})} \frac{F(\pm Z, \varepsilon_e) E_e p_e \varepsilon_\nu^2}{2\gamma^3(1+u)(1-u^2)}, \tag{13}$$

(γ denotes the known Lorentz factor) where m_e, E_e, and p_e are the mass, energy, and momentum, respectively, of the outgoing electrons (or positrons); (ft) is the known ft value; and $F(\pm Z, \varepsilon_e)$ denotes the Coulomb correction function (Fermi function), which accounts for the electromagnetic interaction between the emitted e^- (or e^+) and the charge distribution of the daughter nucleus (final state interaction). In the present work, for the light nuclear system ^{6}He we used the nonrelativistic expression of the Fermi function [36]. For heavier nuclei, however, one needs to explicitly take the final state interaction into consideration and one may use, for example, the distorted wave Born approximation (DWBA) treatment [62].

For the simulations of our present study, we employ the energy spectra of the antineutrinos $\widetilde{\nu}_e$ emitted from β^--radioactive $^6_2$He ions according to the reaction

$$^6_2\text{He} \to {}^6_3\text{Li} + e^- + \widetilde{\nu}_e. \tag{14}$$

Another potential β^--radioactive isotope for $\widetilde{\nu}_e$ beams is $^8_3$Li, while an interesting β^+-radioactive ion source to be accelerated for producing ν_e beams is $^{18}_{10}$Ne, which decays according to the reaction [27,31]

$$^{18}_{10}\text{Ne} \to {}^{18}_{9}\text{F} + e^+ + \nu_e. \tag{15}$$

For ν_e beams another promising β^+-radioactive isotope is $^8_4$B. From the aforementioned potential β-beam targets, $^6_2$He and $^{18}_{10}$Ne have rather low Q values, $Q_{\text{He}} = 3.5$ MeV and $Q_{\text{Ne}} = 3.4$ MeV, respectively (they are good choices for short baseline), while $^8_3$Li and $^8_4$B have relatively high Q values, $Q_{\text{B}} = 13.9$ MeV and $Q_{\text{Li}} = 13.0$ MeV, respectively (they are the best choices for a large baseline) [44]. Energy spectra of the reaction (14) for several integer γ-boost factors ($\gamma = 3, 4, \ldots, 15$) are shown in Fig. 1.

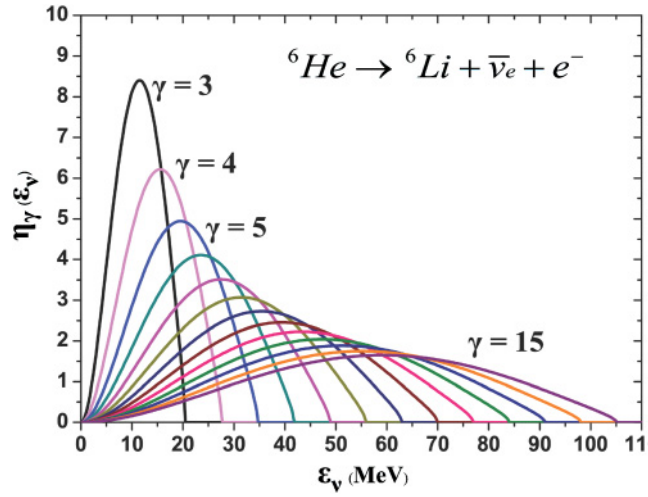

FIG. 1. (Color online) Boosted β-beam antineutrino spectra generated by accelerating β-radioactive ions of $^6_2$He. We have chosen integer Lorentz factors, $\gamma = 3, 4, \ldots, 13$, in Eq. (13).

By exploiting low-energy β-beam spectra of the form of Eq. (13), corresponding to different boost velocities (γ factors), one could construct normalized synthetic neutrino energy distributions $\eta_{bb}(\varepsilon_\nu)$ given by linear combinations as [30,33]

$$\eta_{bb}(\varepsilon_\nu) = \sum_{j=1}^{N} \alpha_j \eta_{\gamma_j}(\varepsilon_\nu), \tag{16}$$

where N is the number of different γ-boosted spectra included in the synthetic spectrum. Such combinations $\eta_{bb}(\varepsilon_\nu)$ are used in Sec. IV to fit original supernova neutrino spectral distributions, $\eta_{\rm SN}(\varepsilon_\nu)$, reaching terrestrial detectors by adjusting the weight parameters α_j through the minimization procedure described in Sec. V [33].

B. Energy spectra of low-energy astrophysical neutrinos

In this subsection, we summarize briefly the basic features of the three extremely interesting low-energy astrophysical neutrino sources: solar, supernova, and geoneutrinos, focusing on their energy distributions, which drop in the neutrino energy range of our original cross sections [7]. We emphasize the supernova neutrino spectra used in the folding procedure in Sec. IV.

The solar neutrino spectra, produced through weak, electromagnetic, and strong nuclear processes in the interior of the Sun, depend not only on the pertinent nuclear processes, but also on the densities and temperatures in the Sun's environment; therefore, the solar ν detection by terrestrial experiments provides unique information about the interior of the Sun and excellent probes for astrophysics, nuclear physics, and particle physics searches. They are ν_e neutrinos distributed in a rather wide energy region, $0.1\ {\rm MeV} \leqslant \varepsilon_\nu \leqslant 18\ {\rm MeV}$, produced either via the well-studied pp-chain reactions or via the CNO-cycle processes. For the solar ν energy spectra and solar ν fluxes the reader is referred, e.g., to recent reviews [1,16,49].

Geoneutrinos are $\tilde{\nu}_e$ antineutrinos produced from β^- decays of natural radioactive elements (predominantly ^{40}K and nuclides in the ^{238}U and ^{232}Th chains) mainly in the crust and mantle of the Earth. They are direct messengers of the abundance and matter distribution of radioactive elements deep within our planet, information that provides strong constraints on several processes that occur inside it [25]. Concerning the energy distribution of geoneutrinos, up to now little is known due to the fact that this is a new rather unknown research field, but in the near future experiments like, e.g., LENA [43,44], SNO+ [42], and others [25], having in their objectives to explore geoneutrinos, are expected to provide us with new data. From the currently known information [18] we imply that their energy range is $0 \leqslant \varepsilon_\nu \leqslant 10$ MeV. As we have seen in Ref. [7], the response of the Te isotopes in the particle-bound excitation region, which coincides with the energy range of geoneutrinos, is rather rich and this motivates similar calculations for other promising and more practical nuclear isotopes (e.g., Xe isotopes) [62].

1. Energy distributions of supernova neutrinos

The neutrino fluxes and the spectra formation in a supernova, according to predictions of recent numerical simulations, are very complicated phenomena [12,57,58]. In essence, the shape of energy distributions of SN neutrinos is determined by the conditions under which the neutrinos are emitted from the star causing the cooling of the protoneutron star formed in the center of the collapsing star [11,13,15,20,45,46]. A thermal spectrum (with the temperature reflecting the conditions at the site where neutrinos decouple) was intuitively employed in earlier studies to describe the SN neutrino energy distribution [47], but modern stellar evolution simulations showed that several effects modify the spectral shape from a purely thermal one (black-body shape) [12,46].

In the stellar environment, the reaction cross sections of the (anti)neutrinos with nuclei which depend on the ν energy, flavor, and helicity play a crucial role in ν spectra formation. In point of fact, due to the small mass of $e^\pm$ in charged current ν-nucleus reactions, the ν_e neutrinos and $\tilde{\nu}_e$ antineutrinos interact with the star's matter via both charged- and neutral-current processes (the proton density pertinent to $\tilde{\nu}_e$ is less than the neutron density determining the interaction of ν_e). The other neutrino flavors, due to the heavy mass of $\mu^\pm$ and $\tau^\pm$, interact only via neutral-current interactions. Generally speaking, for all (anti)neutrino flavors, the energies lie in the range of a few to a few tens of MeV, even though some calculations of ν transport using different opacities lead to somewhat different spectra [57,58].

Recent stellar modeling but also ν-detection terrestrial experiments use analytic expressions that include various modulation effects by inserting a chemical potential μ as the well-known two-parameter Fermi-Dirac (FD) distribution [12]

$$\eta_{\rm FD}(T, n_{\rm dg}; \varepsilon_\nu) = F(n_{\rm dg}) \frac{1}{T^3} \frac{\varepsilon_\nu^2}{1 + e^{(\varepsilon_\nu/T - n_{\rm dg})}}, \tag{17}$$

where T (in MeV) and $n_{\rm dg} = \mu/T$ are the temperature and the degeneracy parameter, respectively, while the constant $F(n_{\rm dg})$ results from the normalization of the distribution (see the Appendix). By inserting $n_{\rm dg}$ the width of the spectrum becomes more narrow compared to the purely thermal shape (pinching effect).

Alternatively, the SN neutrino energy spectrum can also be described with the analytically simpler two-parameter PL energy distribution of the form [12,57,58]

$$\eta_{\rm PL}(\langle\varepsilon_\nu\rangle, \alpha; \varepsilon_\nu) = C(\alpha) \left(\frac{\varepsilon_\nu}{\langle\varepsilon_\nu\rangle}\right)^\alpha e^{-(\alpha+1)(\varepsilon_\nu/\langle\varepsilon_\nu\rangle)}, \tag{18}$$

where $\langle\varepsilon_\nu\rangle$ is the average neutrino energy (equal to the mean energy of the distribution) and the parameter α adjusts the width of the distribution (pinching parameter). The normalization factor $C(\alpha)$ of the PL distribution is derived in the Appendix where explanations of other parameters are included.

Both the FD and PL parametrizations yield very similar distributions characterized by the temperature T or the average energy $\langle\varepsilon_\nu\rangle$ and the width of the spectrum defined as

$$w = \sqrt{\langle\varepsilon_\nu^2\rangle - \langle\varepsilon_\nu\rangle^2}/w_0, \tag{19}$$

where $w_0 = \langle\varepsilon_\nu\rangle/\sqrt{3}$ is the width of the identical FD and PL distributions (see the Appendix). The width of the spectrum w

is characterized by the parameter n_{dg} or α (as w increases n_{dg} or α decrease) and it influences its high-energy tail [57,59].

In Fig. 2, we plot some FD and PL distributions needed for the purposes of the present work (for others see Ref. [33]). In each of the panels of Fig. 2, five equivalent FD and PL spectral distributions are shown for the respective parameters described in the caption of this figure [12,57]. As can be seen, as the temperature grows both the maximum of the distribution shifts to greater neutrino energy and its peak becomes smaller. Also, increasing the degeneracy parameter n_{dg} shifts the spectrum to higher energies [12,30,57]. Similarly, from the PL energy distributions illustrated in Fig. 2 for various values of the pinching parameter ($\alpha = 5.1, 3.7, 2.7$) and average energy $\langle\varepsilon_\nu\rangle$ ($\langle\varepsilon_\nu\rangle$ reflects the depth of the stars from where the neutrinos escape) it becomes obvious that, as $\langle\varepsilon_\nu\rangle$ grows, the maximum of the distribution shifts to higher neutrino energy ε_ν [57]. On the other hand, as the width parameter w grows (for the same average energy $\langle\varepsilon_\nu\rangle$), the maximum of the distribution shifts to smaller neutrino energy ε_ν and its peak becomes smaller.

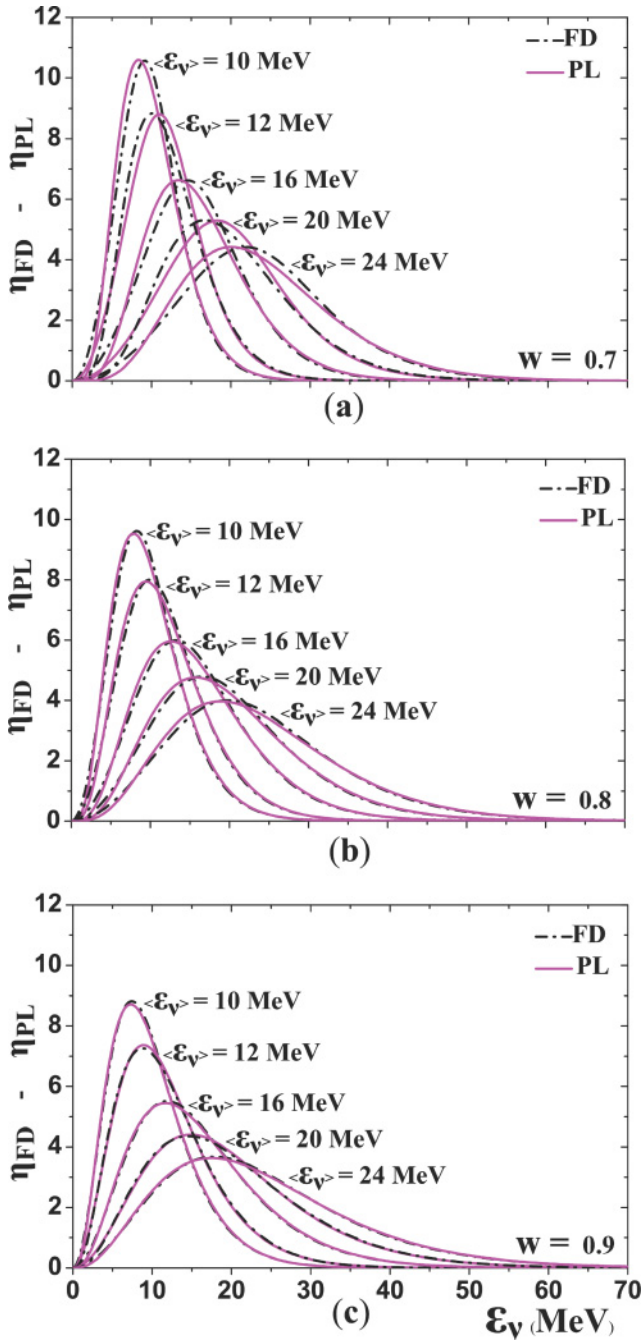

FIG. 2. (Color online) Equivalent Fermi-Dirac (FD) and power-law (PL) ν energy distributions for various values of their parameters. The selected mean-energy values of the PL distribution $\langle\varepsilon_\nu\rangle = 10$, 12, 16, 20, and 24 MeV reflect the depth of the stars from which the neutrinos are escaping. The parameters of equivalent FD distribution are as follows. (a) $w = 0.7$ ($\alpha = 5.1$): $T = 2.14, 2.57, 3.42, 4.28$, and 5.13 MeV ($n_{dg} = 4.4$). (b) $w = 0.8$ ($\alpha = 3.7$): $T = 2.58, 3.10, 4.14$, 5.17, and 6.20 MeV ($n_{dg} = 2.7$). (c) $w = 0.9$ ($\alpha = 2.7$): $T = 2.98$, 3.57, 4.77, 5.96, and 7.15 MeV ($n_{dg} = 1.1$). The above values of temperature T come out of Eq. (A6) [57].

It is worth mentioning that, recently, a Maxwell-Boltzmann type distribution has been proposed for the description of the energy spectra of SN neutrinos [44,62] that approximately resembles the previous ones and has similar advantages (such results are going to be presented elsewhere [62]).

It is important to note that the flavor-dependent fluxes and spectra emitted by supernovae at any distance from the source can be different from those originally produced, which is mainly due to neutrino oscillations but also due to other phenomena [47]. The high statistics neutrino signal from a future galactic SN may allow us to unravel the relevant SN neutrino scenarios.

IV. RESULTS AND DISCUSSION

For the connection of our previous original (double-differential, single-differential, and total) cross section results of neutral-current (anti)neutrino scattering on ^{128,130}Te isotopes [7] with the experiments mentioned in the Introduction, in this section we concentrate on the analysis and the interpretation of neutrino signals potentially measured at the CUORE (detector medium TeO_2) and COBRA (detector medium CdTe or CdZnTe) experiments originating from a future (extra)galactic supernova explosion [18]. Toward this end, to compute folded cross sections through the convolution procedure discussed in Sec. II, at first we employ two-parameter FD and PD distributions as the original energy spectra of supernova neutrinos. Then, we determine synthetic spectra, $\eta_{bb}(\varepsilon_\nu)$, of the form of linear combinations of antineutrino spectra of β^--radioactive ^{6}He ions (boosted with different Lorentz factors γ) by adjusting the weights α_j by fitting them to the original supernova neutrino spectra [30,33,66,67]. Subsequently, these synthetic spectra are used to convolute the total antineutrino cross sections of the reaction $^{130}\text{Te}(\widetilde{\nu}, \widetilde{\nu}')^{130}\text{Te}^*$ (see Sec. IV C).

A. Convoluted double-differential cross sections

In the first step, for the isotopes ^{128,130}Te we evaluate convoluted double-differential cross sections, $[d^2\sigma(\theta, \varepsilon_f)/d\Theta d\varepsilon_f]_{\text{fold}}$, as functions of the outgoing neutrino energy ε_f and the laboratory scattering angle θ given by Eq. (6) [54–56]. We adopt FD and PL spectral distributions for values of the width parameter $w = 0.7$, 0.8, and 0.9 and

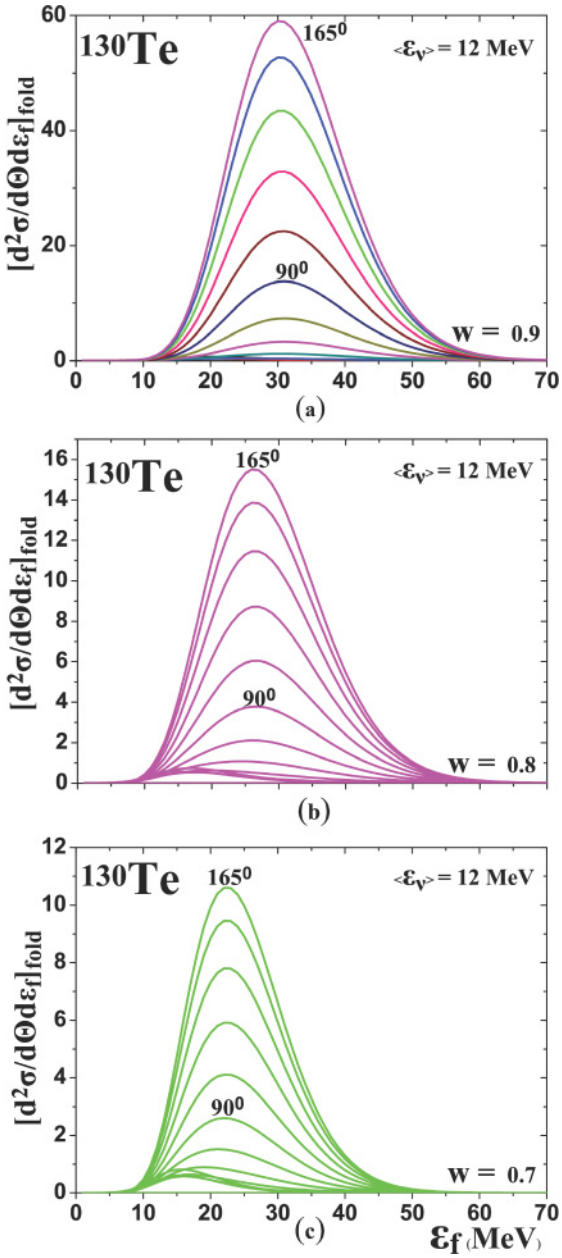

FIG. 3. (Color online) Convoluted double-differential cross sections $[d^2\sigma(\theta, \varepsilon_f)/d\Theta d\varepsilon_f]_{\rm fold}$ ($\times 10^{-40}$ cm^2 MeV^{-1} rad^{-1}) versus the outgoing neutrino energy ε_f for ν scattering on ^{130}Te obtained by using the two-parameter FD distribution with fixed mean neutrino energy $\langle\varepsilon_\nu\rangle = 12$ MeV. The other parameters are (c) $w = 0.7$, $T = 2.57$, and $n_{\rm dg} = 4.4$ ($\alpha = 5.1$); (b) $w = 0.8$, $T = 3.10$, and $n_{\rm dg} = 2.7$ ($\alpha = 3.7$); and (a) $w = 0.9$ $T = 3.58$, and $n_{\rm dg} = 1.1$ ($\alpha = 2.7$). Shown are curves obtained by increasing the laboratory scattering angle θ by $\Delta\theta = 15^\circ$ ($0^\circ < \theta \leqslant 165^\circ$). See the text.

various values of temperature T and average energy $\langle\varepsilon_\nu\rangle$ of the neutrino spectrum.

In Fig. 3, the folded double-differential cross sections of ^{130}Te isotope for the above three values of the width parameter w and fixed mean ν energy in the value $\langle\varepsilon_\nu\rangle = 12$ MeV are illustrated. This mean value, according to the numerical simulations of Refs. [57,58], corresponds to ν_e supernova neutrinos. The temperatures derived from Refs. [57,58] are $T = 2.57$ MeV [Fig. 3(c)], $T = 3.10$ MeV [Fig. 3(b)], and $T = 3.58$ MeV [Fig. 3(a)]. For each set of values $\langle\varepsilon_\nu\rangle$ and α of the PL distribution, in the caption of this figure the values of T and $n_{\rm dg}$ of the equivalent FD distributions are given. Furthermore, in each of the panels of this figure, we varied the laboratory scattering angle θ with a step $\Delta\theta = 15^\circ$ ($0^\circ < \theta \leqslant 165^\circ$).

The results of Fig. 3 show clearly that the high-energy tail of the spectrum plays a significant role in the response of the detector. Decreasing the width w of the SN spectrum, drastically reduces the cross section. In essence, in going from $w = 0.9$ [Fig. 3(a)] to $w = 0.7$ [Fig. 3(c)] the cross section falls by a factor of about 5.5. In addition, as the width is decreasing, the energy maximum of the distribution is shifted to higher values to keep the average energy $\langle\varepsilon_\nu\rangle$ fixed, while the cross section $[d^2\sigma(\theta, \varepsilon_f)/d\Theta d\varepsilon_f]_{\rm fold}$ is decreasing due to suppression of the tail of the distribution.

As can be seen from Fig. 3(a), for $w = 0.9$, in the energy range around the peak, the folded cross section becomes a factor of about 4 larger compared to that for $w = 0.8$ [Fig. 3(b)]. The peak of the response of the ^{130}Te isotope as a potential SN neutrino detector is shifted toward larger energies by about 5 MeV, which implies the existence of a noticeable impact of the supernova neutrino spectra on the signal recorded at the ^{130}Te detector. We have also studied folded cross sections for the ^{128}Te isotope by using the PL distribution, but, as the results are not appreciably different from those of the ^{130}Te isotope, they are not shown here (see Refs. [54,55]).

It is worth mentioning that the results illustrated in Fig. 3 are in excellent qualitative agreement with those of Ref. [63], which refer to charged-current reactions of ν_e neutrinos with much lighter nuclear isotopes (^{12}C, ^{16}O). As mentioned in Sec. II, the recent measurement for a first time of the double-differential cross section $d^2\sigma/d\Omega d\varepsilon_f$ at Fermilab [60,61] (even though in inelastic charged-current ν_μ neutrino scattering on ^{12}C) motivates calculations similar to those of Fig. 3 for other promising nuclear systems too.

B. Convoluted single-differential cross sections

In ν detection by terrestrial experiments, the folded single-differential cross section as a function of the excitation energy $[d\sigma(\omega)/d\omega]_{\rm fold}$, which is known as excitation spectrum induced by the studied ν source on the nuclear detector (here the Te isotopes), is of significant importance and provides a measure of the transmitted neutrino energy in the detector material with which neutrinos interact.

The folded results obtained in the case of the ^{128}Te isotope for the original cross section $d\sigma/d\omega(\omega, \varepsilon_\nu)$ [7] by applying Eq. (7) are illustrated in Fig. 4, where a FD spectral distribution (width parameter $w = 0.8$) was employed for three different values of the mean energy $\langle\epsilon_\nu\rangle = 10$, 16, and 24 MeV. They reflect the neutrino sphere of a collapsing massive star from where ν_e neutrinos ($\langle\epsilon_\nu\rangle = 10$ MeV), $\widetilde{\nu}_e$ antineutrinos ($\langle\epsilon_\nu\rangle = 16$ MeV), and ν_x (anti)neutrinos ($\langle\epsilon_\nu\rangle = 25$ MeV), respectively, are released. We remind the reader that, as can be seen from Eq. (1), the original cross sections are the same for all neutrino (ν_e, ν_μ, ν_τ) or all antineutrino ($\widetilde{\nu}_e$, $\widetilde{\nu}_\mu$, $\widetilde{\nu}_\tau$)

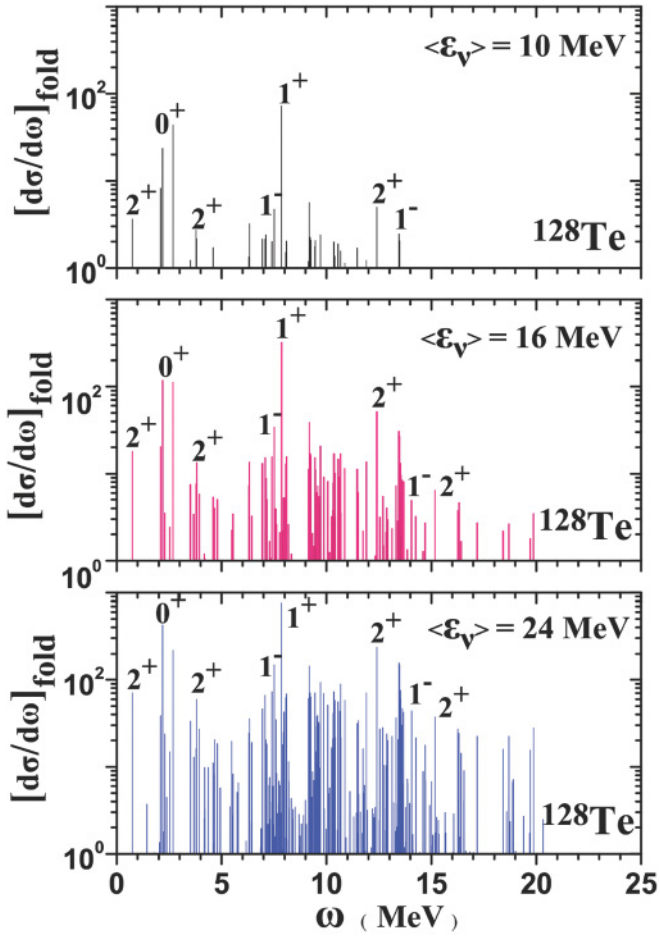

FIG. 4. (Color online) Convoluted single-differential cross section $[d\sigma(\omega)/d\omega]_{\rm fold}$ versus the excitation energy ω ($\times 10^{-40}$ cm^2 MeV^{-1}), averaged over a two-parameter FD spectral distribution ($w = 0.8$, $n_{\rm dg} = 2.7$, or $\alpha = 3.7$) with $\langle\varepsilon_\nu\rangle = 10$ MeV, $T = 2.58$ MeV (upper panel); $\langle\varepsilon_\nu\rangle = 16$ MeV, $T = 4.14$ MeV (middle panel); or $\langle\varepsilon_\nu\rangle = 24$ MeV, $T = 6.20$ MeV (lower panel).

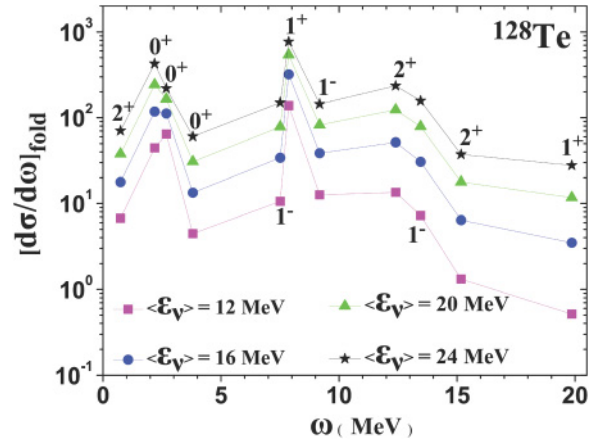

FIG. 5. (Color online) Folded differential cross sections ($\times 10^{-42}$ cm^2 MeV^{-1}) for the reaction ^{128}Te(ν, ν')^{128}Te*, averaged over a FD distribution with width parameter $w = 0.8$ ($n_{\rm dg} = 2.7$) and $T = 3.10$, 4.14, 5.17, and 6.20 MeV. Shown are the corresponding mean energies $\langle\varepsilon_\nu\rangle = 12$, 16, 20, and 24 MeV (the fixed pinching parameter value is $\alpha = 3.7$).

flavors, but for the folded cross sections the chosen values of the parameters determine the ν energy spectrum of a specific flavor [57,58].

From the variation of $[d\sigma(\omega)/d\omega]_{\rm fold}$ through the excitation spectrum of ^{128}Te (see Fig. 4), it is obvious that in all cases there is a rich nuclear response in the range of the discrete spectrum (excitation energy $\omega < 7$–8 MeV), but also in the continuum spectrum. By increasing the mean energy $\langle\epsilon_\nu\rangle$ (or the temperature T) and keeping the width w fixed, the folded cross section $[d\sigma(\omega)/d\omega]_{\rm fold}$ increases drastically throughout the excitation spectrum. Furthermore, by comparing the plots obtained with different values of the width w, we conclude that the effect of the parameter w in increasing the cross section is fairly larger than that of the temperature parameter T (see Ref. [56]).

More specifically in Fig. 4, for inelastic scattering on ^{128}Te by neutrinos with a FD energy distribution with values of the temperature parameter $T = 2.58$ MeV (upper panel), $T = 4.14$ MeV (middle panel), and $T = 6.20$ MeV (lower panel), width parameter $w = 0.8$ (or $n_{\rm dg} = 2.7$ [57,58]), it is clearly demonstrated that the excitation spectrum of SN neutrinos is fragmented over the states. We also see that inelastic ν scattering excites the spin response, which is responsible for the 1^- transitions around 8 and 14 MeV. We furthermore note that the Gamow-Teller strength appears at $\omega = 8$ MeV in good agreement with the results found for ^{208}Pb by Kolbe-Langanke [14]. The enhanced strength of monopole (0^+) and 2^+ transitions has been extensively discussed in Refs. [7,56] for the ^{128,130}Te isotopes and it appears also in the ^{96,98}Mo isotopes (see Refs. [9,10]).

We note that, for the equivalent PL spectra the respective average energies are also given in each panel of Fig. 4 (the pinching parameter is $\alpha = 3.7$ [57,58]). Folded single-differential cross sections $[d\sigma(\omega)/d\omega]_{\rm fold}$ calculated with PL distributions for ^{130}Te are presented in Ref. [56] from where it becomes clear that the folded FD and PL cross sections show the same overall behavior and that the difference between them is fairly small.

In Fig. 5 we examine the influence of the mean energy $\langle\epsilon_\nu\rangle$ of SN neutrino spectra on the response of the ^{128}Te ν detector on some of the most pronounced individual transitions occurring in the original differential cross section of Ref. [7]. As can be seen the increase of the detector response is noticeably larger in the region of high-lying excitations in complete agreement with the results found in Ref. [59], an effect referred to as the supernova thermometer [65].

There are no similar calculations in the literature for the Te isotopes to compare with our present results. Folded cross sections (specifically in the range of the discrete spectrum) are available for a very limited number of nuclear isotopes and they mostly refer to nuclear responses on the continuum spectrum studied by using the continuum RPA or shell model [14,15,36,64].

Before closing this subsection it is worthwhile to make the following comments. As has been stated before, the original cross sections of the transitions induced by neutrino scattering on the studied target nuclei (from their ground state) to both the

particle-bound states and the continuum spectrum have been evaluated by using QRPA [7]. The QRPA continuum spectrum ($\omega \geqslant 10$ MeV for Te isotopes) is constructed by making a discretization of the valence space (separately for protons and neutrons), which implies that the nuclear excitations of neutrino Te reactions for $\omega \geqslant 10$ MeV are represented by discrete states embedded into the continuum spectrum. Obviously, these discrete excited states appear also after folding the original cross sections with a spectral distribution describing the supernova neutrinos (or the neutrino spectra of any neutrino source) as is shown in the excitation spectra of supernova neutrinos in Figs. 4 and 5.

The pronounced peaks of the excitation spectrum of supernova neutrinos shown in Figs. 4 and 5 for $\omega \geqslant 10$ MeV correspond to giant resonances within the continuum nuclear spectrum of ^{128}Te. Similar resonances would appear as superimposed peaks on a rather smooth curve representing the bulk excitation (continuum) spectrum of supernova neutrinos properly described within the context of an appropriate nuclear model (CRPA or Fermi gas model) [65]. Such a picture resembles, e.g., that obtained through continuum RPA calculations based on a Green's function approach [64] that offers a rather realistic description of the continuum nuclear spectrum.

C. SN ν simulations with β-beam ν spectra

The shapes of the β-beam spectra illustrated in Fig. 1 look rather similar to the shapes of the FD and PL distributions and for small Lorentz factors γ ($\gamma \leqslant 15$) their energy range covers that of SN neutrino spectra. As is evident from Eq. (13), their precise shape and average energy are dependent on the boost factor γ of the primary beam and the geometry of the experimental setup (for large γ they are characterized by rather long tails) [27,28,31]. Thanks to these features, the use of β-beam neutrinos in the interpretation of supernova neutrinos was recently proposed [30,33].

In this subsection, the effects of the β-beam properties on the theoretical ν-nucleus cross sections are examined by taking the low-energy β-beam antineutrino spectra of Fig. 1 as an illustrative example. To this purpose, we fold the original total cross sections obtained with QRPA in Ref. [7] for the reaction ^{130}Te$(\widetilde{\nu}, \widetilde{\nu}')^{130}$Te* with synthetic low-energy β-beam antineutrino spectra generated by accelerating β^--radioactive ^{6}He ion beams.

1. Synthetic β-beam spectra based on FD and PL spectral distributions

At first, we adjust the weight parameters α_j that determine the participation of each of the nine γ_j components ($\gamma_1 = 5$, $\gamma_2 = 6, \ldots \gamma_9 = 13$) in the linear combination of Eq. (16), which is the synthetic spectrum $\eta_{bb}(\varepsilon_\nu)$ that simulates an original supernova neutrino energy distribution $\eta_{\rm SN}(\varepsilon_\nu)$. Then, the best fit of $\eta_{bb}(\varepsilon_\nu)$ to the original SN neutrino spectrum $\eta_{\rm SN}(\varepsilon_\nu)$, assuming that this represents the signal recorded at the ^{128,130}Te detectors, results by minimizing the integral [33]

$$\mathcal{Q} = \int_0^\infty \left| \sum_{j=1}^{N} \alpha_j \eta_{\gamma_j(\varepsilon_\nu)} - \eta_{\rm SN}(\varepsilon_\nu) \right| d\varepsilon_\nu. \qquad (20)$$

For the performance of the simulation we employ various SN neutrino spectral distributions. The results of the simulations for the original SN antineutrino spectra described by FD or PL distributions are listed in Tables I and II. The values of the coefficient $\mathcal{Q}$ of Eq. (20), which reflects the quality of the fit coming out of the above simulations, are also listed in these tables. As values of the width parameter w of FD or PL distributions, we utilized $w = 0.8$ (Table I) and $w = 0.9$ (Table II). The mean energies $\langle\varepsilon_\nu\rangle = 16$, 20, and 24 MeV adopted in these tables, according to recent core-collapse supernova studies, cover the mean energies of emitted supernova antineutrinos of all flavors [57,58]. Evidently, the quality of the fit becomes better as the width parameter w increases and this is due to the fact that in the synthetic spectrum the components with large Lorentz factors γ (their width is larger as can be seen from Fig. 1) come out with larger weights α_j. Note that in the synthetic spectrum of Eq. (16) we allow only integer values to contribute [30,33,56,67]. The

TABLE I. Values of the weight coefficients α_j, $j = 1, 2, \ldots, 9$ adjusted by fitting the synthetic spectrum of Eq. (16) (for antineutrinos) to the original SN neutrino spectra described by Fermi-Dirac (FD) and Power-Law (PL) distributions for $w = 0.8$. The resulting quality factors $\mathcal{Q}$ of the fits are also shown [see Eq. (20)]. The values of $\langle\varepsilon_\nu\rangle = 16$, 20, and 24 MeV ($\alpha = 3.7$) and $T = 4.14$, 5.17, and 6.20 MeV ($n_{\rm dg} = 2.7$) describe equivalent PL and FD spectra.

	$\langle\varepsilon_\nu\rangle = 16$ MeV		$\langle\varepsilon_\nu\rangle = 20$ MeV		$\langle\varepsilon_\nu\rangle = 24$ MeV	
α_j	FD	PL	FD	PL	FD	PL
α_1	0.968137	0.963512	0.843445	0.839986	0.555628	0.565200
α_2	0.000007	0.000000	0.000000	0.000004	0.000000	0.034636
α_3	0.009054	0.022860	0.103835	0.089355	0.253795	0.212778
α_4	0.000011	0.000703	0.010720	0.046496	0.086484	0.089183
α_5	0.000223	0.008798	0.013212	0.015173	0.006978	0.053717
α_6	0.000765	0.000271	0.005554	0.006604	0.002004	0.026255
α_7	0.000552	0.000000	0.007661	0.001346	0.094562	0.009053
α_8	0.000077	0.003854	0.001073	0.000390	0.000030	0.006154
α_9	0.021173	0.000000	0.014502	0.000646	0.000521	0.003074
$\mathcal{Q}$	0.511092	0.505723	0.289552	0.261349	0.122564	0.126137

TABLE II. Same as in Table I, but for width parameter $w = 0.9$ ($\alpha = 2.7$). The mean energy values $\langle \varepsilon_\nu \rangle$ are those of Table I and the corresponding temperatures are $T = 4.77$, 5.96, and 7.15 MeV ($n_{\rm dg} = 1.1$).

	$\langle \varepsilon_\nu \rangle = 16$ MeV		$\langle \varepsilon_\nu \rangle = 20$ MeV		$\langle \varepsilon_\nu \rangle = 24$ MeV	
α_j	FD	PL	FD	PL	FD	PL
α_1	0.931640	0.929640	0.694934	0.783812	0.559032	0.581762
α_2	0.000259	0.006255	0.107206	0.000621	0.045297	0.000001
α_3	0.028125	0.042843	0.049977	0.107890	0.174910	0.180461
α_4	0.032710	0.019622	0.014851	0.058568	0.071234	0.099056
α_5	0.001631	0.004942	0.002123	0.028062	0.089175	0.062838
α_6	0.000093	0.002228	0.057580	0.011870	0.024143	0.036351
α_7	0.002544	0.000369	0.070959	0.005939	0.024209	0.020858
α_8	0.000408	0.000354	0.000632	0.000719	0.009977	0.003386
α_9	0.002591	0.000000	0.001738	0.002518	0.002024	0.015283
$\mathcal{Q}$	0.495283	0.488629	0.192084	0.208659	0.071503	0.081421

minimization of the integral in Eq. (20) was achieved by utilizing the optimization algorithm MERLIN [56,66–69].

It is worth mentioning that the values of the quality factor $\mathcal{Q}$ of Tables I and II are much better compared to those found by fitting the neutrino spectra [33,66,67]; this is because of the fine structure of ^{6}He (compared to that of ^{18}Ne employed in Refs. [33,66,67]) and the slightly different behavior of the Fermi function $F(+Z, E_e)$ for β^- processes compared to that of $F(-Z, E_e)$ for β^+ processes. Furthermore, the quality factor $\mathcal{Q}$ is, in general, smaller (better fit) when using PL distributions instead of FD ones and from that point of view PL distributions can be considered as describing with a slightly better accuracy the SN antineutrino energy spectra [33,67]. From Tables I and II, we imply that some fitting coefficients α_j are practically equal to zero, which means that few measurements of β-beam neutrino-nucleus cross sections may be enough in order to reconstruct SN neutrino signals recorded at the nuclear detector [33].

In Fig. 6 the fitting of various synthetic β-beam spectral distributions with nine Lorentz factors γ ($\gamma_1 = 5$, $\gamma_2 = 6, \ldots \gamma_9 = 15$) is demonstrated. We have chosen equivalent FD (upper panel) and PL (lower panel) spectral distributions representing the original supernova neutrino spectra. A conclusion coming out of the simulations of this figure is that, for the same width w, the larger the temperature (in FD) or mean energy (in PL) the better the fit results.

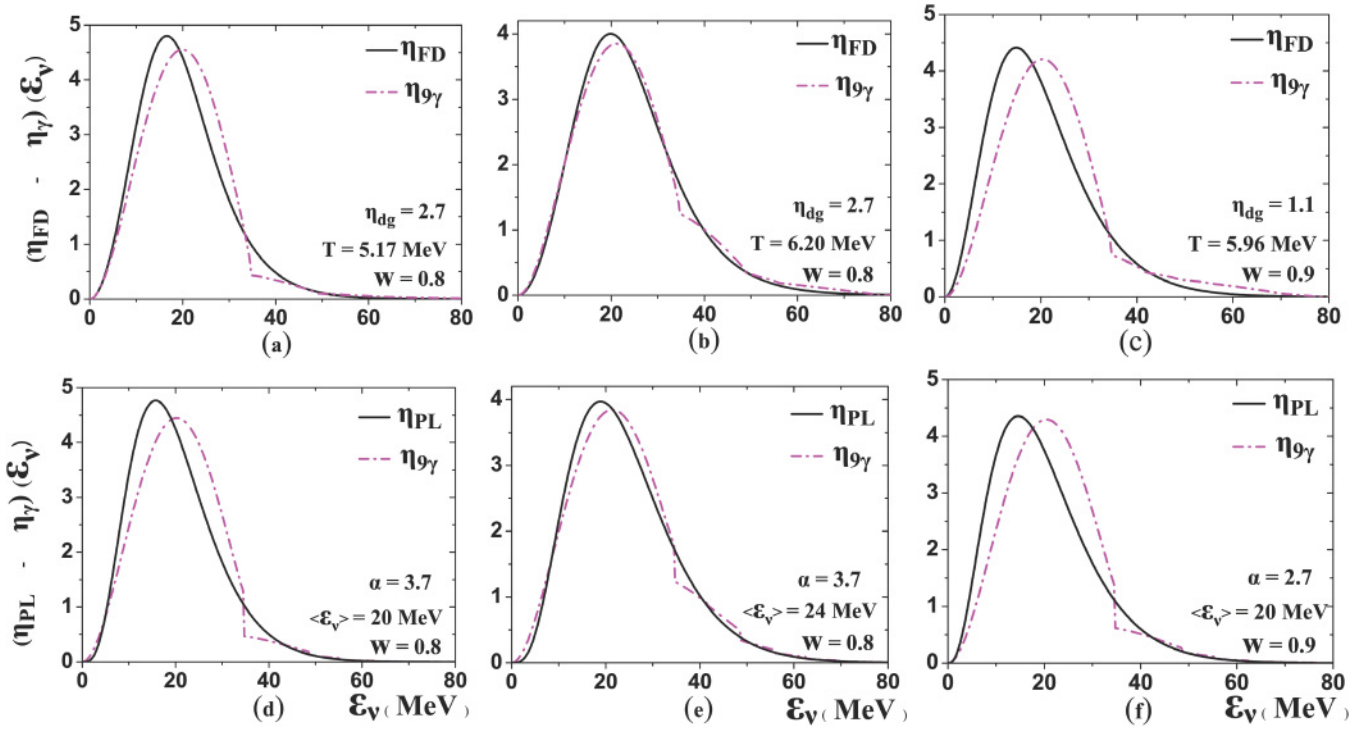

FIG. 6. (Color online) Fitting synthetic β-beam spectral distributions with nine Lorentz factors γ ($\gamma_1 = 5$, $\gamma_2 = 6, \ldots \gamma_9 = 13$) to various FD (upper panels) and PL (lower panels) neutrino energy distributions assuming to represent the original supernova neutrino spectra.

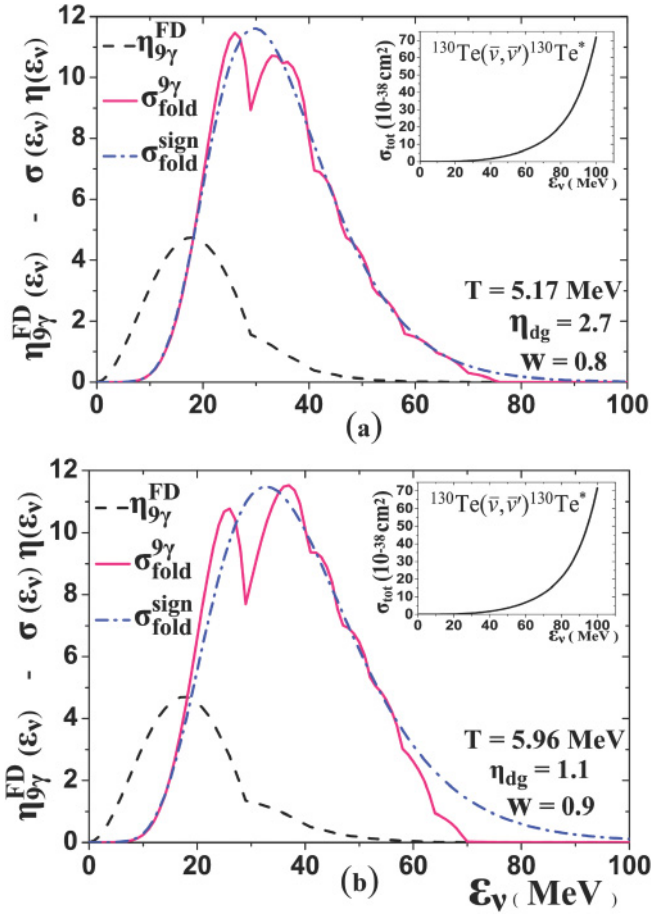

FIG. 7. (Color online) Convoluted total cross sections ($\times 10^{-41}$ cm^2) for ^{130}Te computed by making use of synthetic spectra with nine boost factors $\gamma = 5, 6, \ldots, 13$ (solid line). The response of the assumed original supernova neutrino signals, σ^{sign}_{fold}, are rather well reproduced. The original supernova neutrino spectra $\eta_{FD}(\varepsilon_\nu)$, with $\langle\varepsilon_\nu\rangle = 20$ MeV and width parameter w = 0.8 (a) and w = 0.9 (b), are also illustrated. In the inset we plot the total cross sections of the reaction ^{130}Te$(\widetilde{\nu}, \widetilde{\nu}')^{130}$Te* obtained with the QRPA [7]

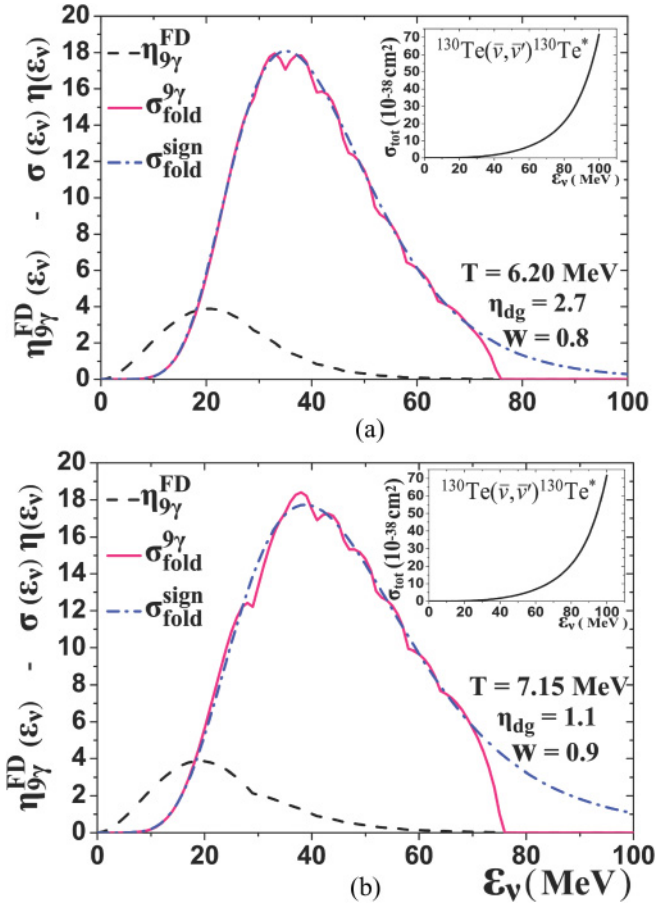

FIG. 8. (Color online) Same as in Fig. 7, but for $\langle\varepsilon_\nu\rangle = 24$ MeV.

2. *Convoluted total cross sections computed with β-beam spectra fitted on SN neutrino signals*

We now consider that an explosion of a (extra)galactic supernova generates a neutrino energy distribution described (at the position of the terrestrial detector) by $\eta^{sign}(\varepsilon_\nu)$. This will yield a total response to the nuclear detector of the form [33]

$$\sigma^{sign}_{fold}(\varepsilon_\nu) = \sigma(\varepsilon_\nu)\eta^{sign}(\varepsilon_\nu), \tag{21}$$

where $\sigma(\varepsilon_\nu)$ is the total cross section of (anti)neutrinos of energy ε_ν scattered on the Te detector. For convenience, $\eta^{sign}(\varepsilon_\nu)$ is considered to be of FD (η_{FD}) or PL (η_{PL}) type distribution.

Assuming that the above response may be simulated by a synthetic spectrum, i.e., by a linear combination of responses to β-beam neutrino spectra with different γ factors, we can write

$$\sigma^{bb}_{fold}(\varepsilon_\nu) = \sum_{j=1}^{N} \alpha_j \sigma(\varepsilon_\nu)\eta_{\gamma_j}(\varepsilon_\nu)\,. \tag{22}$$

In fact, by measuring the nuclear response $\sigma^{sign}_{fold}(\varepsilon_\nu)$ the factors α_j can be determined by fitting σ^{bb}_{fold} to the neutrino signal of Eq. (21). This procedure, known as reconstruction of the supernova neutrino signal [30], is achieved by performing the minimization of Eqs. (16) and (20) for the determination of the factors α_j [33]. Thus, measurement of a spectrum of (extra)galactic SN neutrinos, can determine the components α_j of the synthetic spectrum $\sigma^{bb}_{fold}(\varepsilon_\nu)$, which fit to $\sigma^{sign}_{fold}(\varepsilon_\nu)$. As is demonstrated in Tables I and II, only a few β-beam neutrino measurements are sufficient for a good reconstruction of such a spectrum [30,33].

The theoretical folded cross sections $\sigma^{bb}_{fold}(\varepsilon_\nu) = \sigma^{9\gamma}_{fold}(\varepsilon_\nu)$ for ^{130}Te calculated by using Eq. (22) are compared with the respective signal $\sigma^{sign}_{fold}(\varepsilon_\nu)$ of Eq. (21) in Figs. 7 and 8. In more detail, in these figures the original total cross sections $\sigma(\varepsilon_\nu)$ for the ^{130}Te isotope are folded as is defined in Eq. (22) by using a synthetic spectrum with nine β^--beam components of antineutrino spectra with Lorentz factors $\gamma = 5, 6, \ldots, 13$ (the respective synthetic spectrum $\eta_{bb}(\varepsilon_\nu) = \eta^{FD}_{9\gamma}(\varepsilon_\nu)$ is illustrated by dashed curves in Figs. 7 and 8). We assume that the original supernova neutrino spectra with FD distributions with width parameters $w = 0.8$ [panel (a)] and $w = 0.9$ [panel (b)] generate the signal to the detector shown in Figs. 7 and 8, curves labeled $\sigma^{sign}_{fold}(\varepsilon_\nu)$.

As can be seen, in all cases the peak of the synthetic spectrum, $\eta^{FD}_{9\gamma}(\varepsilon_\nu)$, is located at lower energies compared to

that of the folded cross section $\sigma^{9\gamma}_{\rm fold}(\varepsilon_\nu)$. Also, in all cases the $\sigma^{9\gamma}_{\rm fold}(\varepsilon_\nu)$ reaches its maximum in the high-energy tail of the distribution $\eta^{\rm FD}_{9\gamma}(\varepsilon_\nu)$, i.e., at an energy of $\varepsilon_\nu \approx 35$ MeV for the case of $\langle\varepsilon_\nu\rangle = 20$ MeV and at $\varepsilon_\nu \approx 38$ MeV for the case of $\langle\varepsilon_\nu\rangle = 24$ MeV (the other parameter values are shown in the individual figures). The fit of $\sigma^{9\gamma}_{\rm fold}(\varepsilon_\nu)$ to $\sigma^{9{\rm sign}}_{\rm fold}(\varepsilon_\nu)$ is better for larger mean energies $\langle\varepsilon_\nu\rangle$ (or temperatures T).

In the insets of Figs. 7 and 8, the original results of the total cross section, $\sigma_{\rm tot}(\varepsilon_\nu)$, versus the incoming antineutrino energy ε_ν for the ^{130}Te isotope is illustrated [it is clear that they follow the square dependence on the energy ε_ν as expected from Eq. (1)].

V. SUMMARY AND CONCLUSIONS

Astrophysical neutrinos (solar, supernova, and Earth neutrinos) are key particles in investigating the structure and evolution of stars, astronuclear reactions, and neutrino-driven explosion mechanisms of massive stars, and also in deepening our knowledge on the fundamental interactions and the nuclear weak responses. In this work we applied the convolution procedure to theoretical neutrino-nucleus cross sections obtained previously with realistic nuclear structure calculations (QRPA method) to compute folded cross sections through specific spectral distributions describing supernova neutrino energy spectra.

The convoluted (double-differential, $d^2\sigma/d\Omega d\omega$, single-differential, $d\sigma/d\omega(\omega)$, and total, $\sigma_{\rm tot}$) cross sections reflect the neutrino signals generated at the selected terrestrial detectors (^{128,130}Te) from specific ν sources and our present results demonstrate clearly the weak responses to low-spin multipoles (1^-, 1^+, 0^+, 2^+) generated by supernova neutrino spectra. The excitation spectra of ^{128,130}Te isotopes, contents of the CUORE and COBRA detector medium, show rich responses in the energy range $\omega \preccurlyeq 20$ MeV, which is relevant for low- and intermediate-energy supernova neutrinos but also for solar and Earth neutrinos.

We also obtained a reliable description of the responses of ^{128}Te and ^{130}Te isotopes to various β-beam neutrino energy spectra and found that the folded cross sections for neutral-current neutrino scattering processes show a smooth behavior as functions of the γ boosting factor of the β-beam spectra originated from accelerated ^{6}He ions, which implies that the overall γ dependence of the folded cross sections may be reproduced by a limited number of measurements.

Precious information for the understanding of the isospin and spin-isospin nuclear responses studied in this paper, neutrino physics, the fundamental weak interactions, and specifically the supernova dynamics can be obtained by future low-energy β beams or spallation neutron sources. Toward this purpose, pursuing theoretical neutrino scattering studies at low energies as we did in the present work may be essential in unraveling unknown properties and the role of neutrinos in a plethora of open neutrino physics issues.

ACKNOWLEDGMENTS

VT is grateful to Professor J. D. Vergados for fruitful discussions. TSK wishes to thank K. Langanke and J. Wambach for stimulating discussions. This research was supported by the ΠΕΝΕΔ Project No. 03EΔ807 of the General Secretariat for Research and Technology of the Hellenic Ministry of Development and the Helmholtz International Center for the Facility for Anti-proton and Ion Research (HIC for FAIR) within the framework of the LOEWE Program.

APPENDIX

1. The terms $\mathcal{C}_V$, $\mathcal{C}_A$, and $\mathcal{C}_{VA}$

The term $\mathcal{C}_V$ ($\mathcal{C}_A$) in Eq. (1) is a summation over the contributions coming from the polar-vector (axial-vector) multipole operators as [7]

$$\mathcal{C}_{V(A)} = \sum_{J=0}^{\infty}\left|\langle J_f\|\widehat{M}^{(5)}_J(q) + \frac{\omega}{q}\widehat{L}^{(5)}_J(q)\|J_i\rangle\right|^2 + \sum_{J=1}^{\infty}\left(-\frac{q_\mu^2}{2q^2} + \tan^2\frac{\theta}{2}\right)\left[\left|\langle J_f|\left|\widehat{T}^{\rm mag(5)}_J(q)\right||J_i\rangle\right|^2 + \left|\langle J_f|\left|\widehat{T}^{\rm el(5)}_J(q)\right||J_i\rangle\right|^2\right]. \quad \text{(A1)}$$

The definitions of the eight multipole operators $\widehat{M}^{(5)}_J$, $\widehat{L}^{(5)}_J$, $\widehat{T}^{\rm el(5)}_J$, and $\widehat{T}^{\rm mag(5)}_J$, where the superscript '5' refers to the axial-vector components of the hadronic current, are given in Refs. [7–9].

The interference term $\mathcal{C}_{VA}$ in Eq. (1) contains the product of transverse polar-vector and transverse axial-vector matrix elements as

$$\mathcal{C}_{VA} = 2\tan\frac{\theta}{2}\left[-\frac{q_\mu^2}{q^2} + \tan^2\frac{\theta}{2}\right]^{1/2} \times \sum_{J=1}^{\infty}{\rm Re}e\langle J_f|\left|\widehat{T}^{\rm mag}_J(q)\right||J_i\rangle\langle J_f|\left|\widehat{T}^{\rm el}_J(q)\right||J_i\rangle^*. \quad \text{(A2)}$$

Obviously, for normal parity transitions, $\mathcal{C}_{VA}$ contains contributions of $\widehat{T}^{\rm el}_J$ and $\widehat{T}^{\rm mag5}_J$ operators while for abnormal parity ones it contains matrix elements of $\widehat{T}^{\rm mag}_J$ and $\widehat{T}^{\rm el5}_J$ [7–9]. For additional details see Ref. [7].

2. Fermi-Dirac energy distribution

By introducing the degeneracy parameter $n_{\rm dg}$ (the chemical potential μ divided by the temperature T, $n_{\rm dg} = \mu/T$), the FD energy distribution is written as [12,13]

$$\eta_{\rm FD}(T, n_{\rm dg}; x) = F(n_{\rm dg})\frac{1}{T}\frac{x^2}{1+e^{(x-n_{\rm dg})}}, \quad x = \frac{\varepsilon_\nu}{T}. \quad \text{(A3)}$$

The width of the latter spectrum is reduced compared to the corresponding thermal one (pinching effect). The normalization constant $F(n_{\rm dg})$ of the distribution depends on the degeneracy parameter $n_{\rm dg}$ and it is given by the relation

$$\frac{1}{F(n_{\rm dg})} = \int_0^\infty \frac{x^2}{e^{x-n_{\rm dg}}+1}dx. \quad \text{(A4)}$$

By inserting Eq. (A4) into Eq. (A3), the normalized FD spectral distribution reads

$$\eta_{\rm FD}(T, n_{\rm dg}; \varepsilon_\nu) = \left[\int_0^\infty \frac{x^2}{e^{x-n_{\rm dg}}+1}dx\right]^{-1} \frac{\left(\varepsilon_\nu^2/T^3\right)}{1+e^{(\varepsilon_\nu/T-n_{\rm dg})}}. \tag{A5}$$

The mean energy $\langle\varepsilon_\nu\rangle$ of the neutrinos described by the latter distribution is written in terms of T and $n_{\rm dg}$ as [52,57]

$$\langle\varepsilon_\nu\rangle = (3.1514 + 0.1250\, n_{\rm dg} + 0.0429\, {n_{\rm dg}}^2 + \cdots)T. \tag{A6}$$

As can be easily proved, for $n_{\rm dg} = 0$ (thermal shape or blackbody shape distribution), $F(0) = 7\pi^4/120 \sim 5.68$ [57].

3. Power-law energy distribution

Recently it was found [57] that the SN neutrino energy spectra can be fitted by using a PL energy distribution of the form

$$\eta_{\rm PL}(\langle\varepsilon_\nu\rangle, \alpha; \varepsilon_\nu) = C(\alpha)\left(\frac{\varepsilon_\nu}{\langle\varepsilon_\nu\rangle}\right)^\alpha e^{-(\alpha+1)(\varepsilon_\nu/\langle\varepsilon_\nu\rangle)}, \tag{A7}$$

where $\langle\varepsilon_\nu\rangle$ is the neutrino average energy and the parameter α adjusts the width of the spectrum. The factor $C(\alpha)$ is computed from the normalization condition, which reads

$$\frac{1}{C(\alpha)} = \int_0^\infty \left(\frac{\varepsilon_\nu}{\langle\varepsilon_\nu\rangle}\right)^\alpha e^{-(\alpha+1)(\varepsilon_\nu/\langle\varepsilon_\nu\rangle)} d\varepsilon_\nu. \tag{A8}$$

From the latter equation we find

$$C(\alpha) = \frac{(\alpha+1)^{\alpha+1}}{\Gamma(\alpha+1)\langle\varepsilon_\nu\rangle}; \tag{A9}$$

therefore, the normalized PL distribution is written as

$$\eta_{\rm PL}(\langle\varepsilon_\nu\rangle, \alpha; \varepsilon_\nu) = \frac{(\alpha+1)^{\alpha+1}}{\Gamma(\alpha+1)} \frac{\varepsilon_\nu^\alpha}{\langle\varepsilon_\nu\rangle^{\alpha+1}} e^{-(\alpha+1)(\varepsilon_\nu/\langle\varepsilon_\nu\rangle)}. \tag{A10}$$

We note that the average energy of the PL distribution is always equal to the mean energy $\langle\varepsilon_\nu\rangle$.

4. Identical Fermi-Dirac and power-law distributions for $n_{\rm dg} = -\infty$ and $\alpha = 2$

Equation (A5) can also be written as

$$\eta_{\rm FD}(T, n_{\rm dg}; \varepsilon_\nu) = \left[\int_0^\infty \frac{x^2}{e^x+e^{n_{\rm dg}}}dx\right]^{-1} \frac{\left(\varepsilon_\nu^2/T^3\right)}{e^{(\varepsilon_\nu/T)}+e^{n_\alpha}}. \tag{A11}$$

The latter equation for $n_{\rm dg} = -\infty$ becomes

$$\eta_{\rm FD}(T, n_{\rm dg} = -\infty; \varepsilon_\nu) = \frac{\varepsilon_\nu^2}{2T^3} e^{-(\varepsilon_\nu/T)}. \tag{A12}$$

Also, Eq. (A10) for $\alpha = 2$ yields

$$\eta_{\rm PL}(\langle\varepsilon_\nu\rangle, \alpha = 2; \varepsilon_\nu) = \frac{27}{2} \frac{\varepsilon_\nu^2}{\langle\varepsilon_\nu\rangle^3} e^{-3\varepsilon_\nu/\langle\varepsilon_\nu\rangle}. \tag{A13}$$

By comparing Eqs. (A12) and (A13), we conclude that the equality (identical spectra) holds if $T = \langle\varepsilon_\nu\rangle/3$, a relation which applies when neutrinos are considered as nondegenerate particles.

The width of the identical FD and PL distributions is $w_0 = \langle\varepsilon_\nu\rangle/\sqrt{3}$. For other equivalent spectra, see Ref. [57].

[1] H. Ejiri, Phys. Rep. **338**, 265 (2000).
[2] E. Kolbe and T. S. Kosmas, Springer Trac. Mod. Phys. **163**, 199 (2000).
[3] J. D. Vergados, Phys. Rep. **361**, 1 (2002).
[4] K. Langanke, Acta Phys. Pol. B **39**, 265 (2008).
[5] E. Kolbe, Phys. Rev. C **54**, 1741 (1996).
[6] T. S. Kosmas and E. Oset, Phys. Rev. C **53**, 1409 (1996).
[7] V. Tsakstara and T. S. Kosmas, Phys. Rev. C **83**, 054612 (2011).
[8] T. W. Donnelly and R. D. Peccei, Phys. Rep. **50**, 1 (1979).
[9] V. C. Chasioti and T. S. Kosmas, Nucl. Phys. A **829**, 234 (2009).
[10] K. G. Balasi, E. Ydrefors, and T. S. Kosmas, Nucl. Phys. A **868-869**, 82 (2011).
[11] H. A. Bethe, Rev. Mod. Phys. **62**, 801 (1990).
[12] H.-T. Janka and W. Hillebrandt, Astron. Astrophys. **224**, 49 (1989).
[13] H.-T. Janka and B. Mueller, Phys. Rep. **256**, 135 (1995).
[14] E. Kolbe and K. Langanke, Phys. Rev. C **63**, 025802 (2001).
[15] K. Langanke and G. Martinez-Pinedo, Rev. Mod. Phys. **75**, 819 (2003).
[16] J. D. Vergados and H. Ejiri, Nucl. Phys. B **804**, 144 (2008).
[17] J. D. Vergados, F. T. Avignone, and I. Giomataris, Phys. Rev. D **79**, 113001 (2009).
[18] J. D. Vergados, J. Phys. Conf. Ser. **309**, 012031 (2011).
[19] K. Langanke, in *Solar, Stellar and Galactic Connections between Particle Physics and Astrophysics*, edited by A. Carraminana *et al.* (Springer, Heidelberg, 2007), pp. 341.
[20] H.-Th. Janka, K. Langanke, A. Marek, G. Martinez-Pinedo, and B. Mueller, Phys. Rep. **442**, 38 (2007).
[21] Y. Giomataris and J. D. Vergados, Phys. Lett. B **634**, 23 (2006).
[22] J. D. Vergados and Y. Giomataris, Phys. Atom. Nucl. **70**, 140 (2007).
[23] Borexino Collaboration, Astropart. Phys. **16**, 205 (2002).
[24] S. Abe *et al.* (KamLAND Collaboration), Phys. Rev. Lett. **100**, 221803 (2008).
[25] Borexino Collaboration, Phys. Lett. B **687**, 299 (2010).
[26] P. Zucchelli, Phys. Lett. B **532**, 166 (2002).
[27] C. Volpe, J. Phys. G **30**, L1 (2004).
[28] J. Serreau and C. Volpe, Phys. Rev. C **70**, 055502 (2004).
[29] G. C. McLaughlin, Phys. Rev. C **70**, 045804 (2004).
[30] N. Jachowicz and G. C. McLaughlin, Phys. Rev. Lett. **96**, 172301 (2006).
[31] C. Volpe, J. Phys. G **34**, R1 (2007).
[32] P. S. Amanik and G. C. McLaughlin, Phys. Rev. C **75**, 065502 (2007).
[33] N. Jachowicz, G. C. McLaughlin, and C. Volpe, Phys. Rev. C **77**, 055501 (2008).

[34] F. T. Avignone and Y. V. Efremenko, Nucl. Phys. B, Proc. Suppl. **87**, 304 (2000).
[35] F. T. Avignone and Y. V. Efremenko, J. Phys. G **29**, 2615 (2003).
[36] E. Kolbe, K. Langanke, G. Martinez-Pinedo, and P. Vogel, J. Phys. G **29**, 2569 (2003).
[37] W. C. Louis, Prog. Part. Nucl. Phys. D **63**, 51 (2009).
[38] J. Alonso *et al.*, arXiv:1006.0260 [physics.ins-det] (2010).
[39] C. Arnaboldi *et al.*, Phys. Rev. C **78**, 035502 (2008).
[40] E. Fiorini, invited talk at MEDEX'2011, Prague, June 13–16, 2011.
[41] K. Zuber, Phys. Lett. B **519**, 1 (2001).
[42] K. Zuber, Prog. Part. Nucl. Phys. **57**, 235 (2006).
[43] G. Fiorentini *et al.*, Phys. Rep. **453**, 117 (2007).
[44] M. Wurm *et al.*, arXiv:1104.5620 [astro-ph.IM] (2011).
[45] C. Fröhlich, G. Martinez-Pinedo, M. Liebendörfer, F.-K. Thielemann, E. Bravo, W. R. Hix, K. Langanke, and N. T. Zinner, Phys. Rev. Lett. **96**, 142502 (2006).
[46] M. Liebendoerfer, M. Rampp, H.-T. Janka, and A. Mezzacappa, Astrophys. J. **620**, 840 (2005).
[47] H. Duan and A. Dighe, Phys. Rev. D **77**, 113002 (2008).
[48] G. Bellini *et al.* (Borexino Collaboration), Phys. Rev. Lett. **107**, 141302 (2011).
[49] B. Aharmim *et al.*, arXiv:1107.2901 [nucl-ex] (2011).
[50] J. W. F. Valle, J. Phys. Conf. Ser. **203**, 012009 (2010); arXiv:1001.5189 [hep-ph] (2010).
[51] V. Tsakstara, T. S. Kosmas, J. Sinatkas, V. C. Chasioti, and P. C. Divari, AIP Conf. Proc. **963**, 1383 (2007).
[52] V. Tsakstara, T. S. Kosmas, V. C. Chasioti, and J. Sinatkas, AIP Conf. Proc. **972**, 562 (2008).
[53] V. Tsakstara, T. S. Kosmas, P. C. Divari, and J. Sinatkas, AIP Conf. Proc. **1180**, 140 (2009).
[54] V. Tsakstara, T. S. Kosmas, and P. C. Divari, J. Phys.: Conf. Ser. **203**, 012093 (2010).
[55] V. Tsakstara, T. S. Kosmas, P. C. Divari, and J. Sinatkas, Prog. Part. Nucl. Phys. **64**, 411 (2010).
[56] V. Tsakstara, Ph.D. thesis, Ioannina University Press, Ioannina, 2010.
[57] M. T. Keil, G. G. Raffelt, and H.-T. Janka, Astrophys. J. **590**, 971 (2003).
[58] G. G. Raffelt, M. T. Keil, R. Buras, H.-T. Janka, and M. Rampp, arXiv:astro-ph/0303226v1 (2003).
[59] N. Jachowicz and K. Heyde, Phys. Rev. C **68**, 055502 (2003).
[60] A. A. Aguilar-Arevalo *et al.* (MiniBooNE Collaboration), Phys. Rev. D **81**, 092005 (2010).
[61] A. A. Aguilar-Arevalo *et al.* (MiniBooNE Collaboration), Phys. Rev. D **81**, 032001 (2010).
[62] V. Tsakstara and T. S. Kosmas (in preparation).
[63] W. C. Haxton, Phys. Rev. D **36**, 2283 (1987).
[64] N. Jachowicz, K. Heyde, and J. Ryckebusch, Phys. Rev. C **66**, 055501 (2002).
[65] N. Jachowicz, S. Rombouts, K. Heyde, and J. Ryckebusch, Phys. Rev. C **59**, 3246 (1999).
[66] V. Tsakstara and T. S. Kosmas, Prog. Part. Nucl. Phys. **64**, 407 (2010).
[67] V. Tsakstara, T. S. Kosmas, and J. Wambach, Prog. Part. Nucl. Phys. **66**, 424 (2011).
[68] I. E. Lagaris, A. Likas, and D. Fotiadis, Comput. Phys. Commun. **104**, 1 (1997).
[69] T. S. Kosmas and I. E. Lagaris, J. Phys. G **28**, 2907 (2002).